NASA TECHNICAL NOTE

NASA TN D-1927

NASA TN D-1927

A COMPARISON OF THE THEORETICAL AND EXPERIMENTAL STAGNATION-POINT HEAT TRANSFER IN AN ARC-HEATED SUBSONIC STREAM

by Ronald D. Brown

Langley Research Center
Langley Station, Hampton, Va.

NATIONAL AERONAUTICS AND SPACE ADMINISTRATION • WASHINGTON, D. C. • JUNE 1964

A COMPARISON OF THE THEORETICAL AND EXPERIMENTAL STAGNATION-POINT HEAT TRANSFER IN AN ARC-HEATED SUBSONIC STREAM

By Ronald D. Brown

Langley Research Center
Langley Station, Hampton, Va.

NATIONAL AERONAUTICS AND SPACE ADMINISTRATION

For sale by the Office of Technical Services, Department of Commerce,
Washington, D.C. 20230 -- Price $0.75

NATIONAL AERONAUTICS AND SPACE ADMINISTRATION

TECHNICAL NOTE D-1927

A COMPARISON OF THE THEORETICAL AND EXPERIMENTAL STAGNATION-POINT HEAT TRANSFER IN AN ARC-HEATED SUBSONIC STREAM

By Ronald D. Brown

SUMMARY

Stagnation-point heat-transfer measurements on flat-face cylinders of three different diameters in a 6-inch subsonic arc tunnel do not follow the laminar heat-transfer theory of Fay and Riddell for the Reynolds number range covered in this report. It was concluded that the difference between theory and experiment was not a result of changes in velocity gradient associated with compressibility or channel-blocking effects. The deviation from laminar-flow theory is attributed to the free-stream turbulence in the test medium that is caused by the a-c electric arcs in arc chamber of subsonic arc tunnel.

INTRODUCTION

Currently, electric arc-heated facilities are being used to simulate the aerodynamic heating during atmospheric reentry for structures and material tests. Many of these arc-jet facilities are subsonic. The theoretical heat-transfer relationships of Fay and Riddell (ref. 1) should be applicable to the test conditions typical of such subsonic arc facilities provided the proper stagnation-point velocity gradients are used. Some early tests in some of the large subsonic arc facilities at Langley Research Center indicate that the experimentally measured stagnation-point heat-transfer rates differ from those calculated theoretically. Therefore, a systematic series of tests have been conducted in the 6-inch subsonic arc tunnel (ref. 2) at Langley Research Center in order to determine the reasons for these discrepancies. In order to evaluate properly the stagnation-point velocity gradient required in the Fay and Riddell heat-transfer expression, the theoretical effects of compressibility and channel blocking are considered. These theoretical stagnation-point velocity gradients are evaluated in terms of measurable quantities that can be obtained for any subsonic high-temperature facility.

Stagnation-point heat-transfer measurements were made on three flat-face cylinders with different diameters and on a 3-inch-diameter hemisphere-cylinder in a subsonic arc tunnel. This facility utilizes a three-phase a-c power supply with water-cooled copper electrodes to heat the test medium (in this case, air). The free-stream temperatures, free-stream pressures, the stagnation-point heat-transfer rates, and heat-transfer distributions were determined at several operating conditions. An empirical heat-transfer relationship, utilizing non-dimensional parameters, is derived from the experimental data.

SYMBOLS

A	area, sq ft
c_p	specific heat at constant pressure, Btu/lb-^{o}R
D	diameter, ft
h	enthalpy, Btu/lb
K	wall effect factor defined by equation (18)
k	thermal conductivity, Btu/ft-sec-^{o}R
M	Mach number
N_{Pr}	Prandtl number, $\frac{c_p\mu}{k}$
N_{Re}	Reynolds number based on body diameter, $\frac{\rho u D}{\mu}$
N_{St}	Stanton number, $\frac{\dot{q}}{\rho u(h_s - h_w)}$
p	pressure, lb/sq ft
$\dot{q}$	heat-transfer rate, Btu/ft^2-sec
R	radius, ft
t	time, sec
T	temperature, ^{o}R
u	velocity, ft/sec
$\dot{w}$	tunnel air-flow rate, lb/sec
x	surface distance from stagnation point, ft

Z	compressibility factor
β	velocity gradient, per sec
θ	spherical coordinate
λ	ratio of model diameter to stream diameter
μ	viscosity, lb-sec/sq ft
ρ	density, lb/ft^3
τ	thickness, ft
φ	velocity potential, sq ft/sec

Subscripts and component designations:

b	body
e	edge
ex	experimental
f	face
ff	flat-face
hs	hemispherical
o	incompressible
s	stagnation
th	theoretical
w	wall
∞	free-stream condition

THEORY

General Heat-Transfer Expressions

A theory for the heat transfer at the stagnation point in a dissociated gas is discussed in detail by Fay and Riddell in reference 1. The general stagnation-point heat-transfer expression for equilibrium laminar flow (from ref. 1) with a Lewis number of 1.0 is as follows:

$$\dot{q}_s = \frac{0.76}{N_{Pr,w}^{0.6}}\left(\rho_s\mu_s\right)^{0.4}\left(\rho_w\mu_w\right)^{0.1}\left(h_s - h_w\right)\left(\frac{du_e}{dx}\right)_{x=0}^{0.5} \tag{1}$$

where

$$\left(\frac{du_e}{dx}\right)_{x=0} = \beta \tag{2}$$

Equation (2) is introduced into equation (1) in a nondimensional form to yield

$$\dot{q}_s = \frac{0.76}{N_{Pr,w}^{0.6}}\left(\rho_s\mu_s\right)^{0.4}\left(\rho_w\mu_w\right)^{0.1}\left(h_s - h_w\right)\left(\frac{\beta D}{u_\infty}\right)^{0.5}\left(\frac{u_\infty}{D}\right)^{0.5} \tag{3}$$

the Stanton number is here defined as

$$N_{St,s} = \frac{\dot{q}_s}{\rho_s u_\infty (h_s - h_w)} \tag{4}$$

which can be written in the following form by substituting equation (3) into equation (4):

$$N_{St,s} = 0.76 N_{Pr,w}^{-0.6} N_{Re}^{-0.5}\left(\frac{\beta D}{u_\infty}\right)^{0.5}\left(\frac{\rho_w\mu_w}{\rho_s\mu_s}\right)^{0.1} \tag{5}$$

This nondimensional representation of the stagnation-point heat-transfer rate is a convenient form for data analysis. The evaluation of the nondimensional stagnation-point velocity gradient $\beta D/u_\infty$ is considered in the following sections.

Stagnation-Point Velocity Gradient

Sphere.- In a uniform stream of infinite diameter, the flow at the surface of a sphere of radius R is given by the velocity potential function (ref. 3):

$$\varphi_o = \frac{3}{2} u_\infty R \cos\theta \tag{6}$$

where along the surface

$$u = -\frac{1}{R}\frac{\partial\varphi_o}{\partial\theta} \tag{7}$$

and the velocity gradient

$$\beta = \left(\frac{\partial u}{\partial x}\right)_{x=0} = -\frac{1}{R}\frac{\partial^2 \varphi_o}{\partial \theta \, \partial x} \tag{8}$$

By utilizing the potential flow function from equation (6), the stagnation-point velocity gradient in nondimensional form for a sphere becomes

$$\frac{\beta D}{u_\infty} = 3 \tag{9}$$

Circular disk.- On a flat-face cylinder, a stagnation-point velocity gradient can be obtained from potential flow theory by assuming that the flat face is a circular disk moving perpendicular to its plane in an infinite-diameter stream. The velocity potential function for this type of configuration is given in reference 4 as

$$\varphi_o = \frac{2}{\pi} u_\infty R \cos\theta \tag{10}$$

By substituting into equation (8), the stagnation-point velocity gradient on a circular disk is as follows:

$$\left(\frac{\beta D}{u_\infty}\right)_{\text{Circular disk}} = \frac{4}{\pi} \tag{11}$$

In reference 5 the stagnation-point velocity gradient was measured experimentally on a flat-face circular cylinder in an open jet. At a low Mach number the experimental velocity gradient on the flat-face circular cylinder approaches the theoretical value of the circular disk as shown in figure 1. Thus, it may be concluded that the velocity gradient for the circular disk is a good approximation of stagnation-point velocity gradient for the flat-face circular cylinder at low Mach numbers.

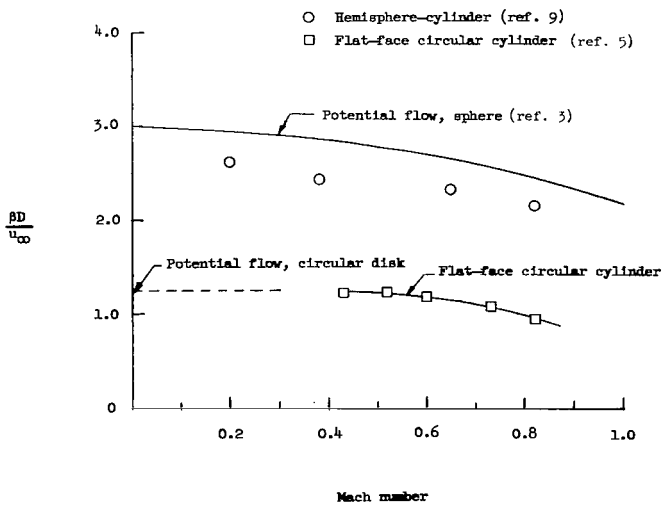

Figure 1.- Velocity gradient as a function of Mach number.

Shape Effect on Heat Transfer

An approximate relationship for the heat-transfer rate on a body whose front face is a spherical segment (see fig. 2) can be obtained by a linear interpolation between the limiting cases of the circular disk and the sphere. A similar linear relationship in reference 6 was obtained experimentally at supersonic Mach numbers. Unpublished data obtained in a different subsonic arc-jet verified that this relationship is linear. Thus, for spherical segments, as shown in figure 2, the heat-transfer relationship is as follows:

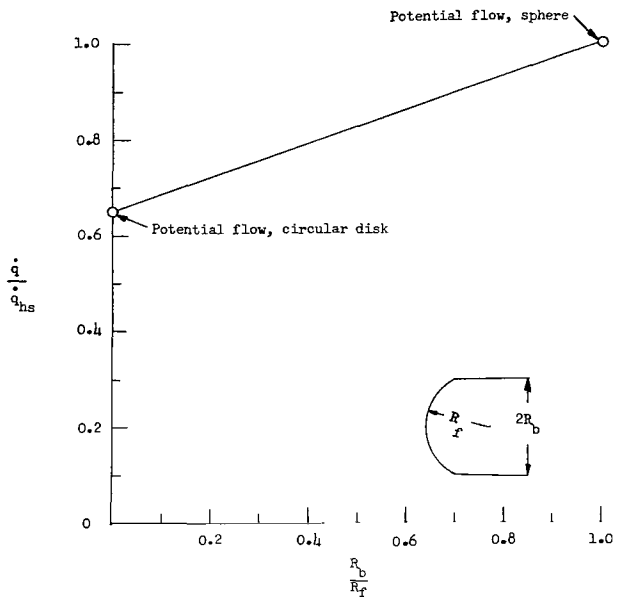

Figure 2.- Heat-transfer ratio as a function of body-to-face radius.

$$\left(\dot{q}_s\right)_{M=0} = \left(\dot{q}_{hs}\right)_{M=0}\left(0.65 + 0.35\,\frac{R_b}{R_f}\right) \tag{12}$$

where $\dot{q}_{hs}$ is the stagnation-point heat-transfer rate on the hemisphere, R_b is the body radius, and R_f is the face radius.

Channel Blocking Effect on Velocity Gradient

In the present series of tests the cross-sectional area of the model was as large as 25 percent of the cross-sectional area of the test section. It is of interest to determine what effect the channel blocking has on the stagnation-point velocity gradient. A theoretical approximation of the channel-blocking effect may be obtained by using the subsonic velocity potential flow theory for the flow past a sphere inside an infinite length cylindrical duct as presented in references 7 and 8.

The incompressible surface-velocity potential function for a sphere inside an infinitely long circular cylinder from reference 8 is:

$$\varphi_o = \frac{\frac{3}{2}\,u_\infty R\cos\theta}{1 - 0.797\lambda^3} \tag{13}$$

where λ is the ratio of the diameter of the sphere to cylinder. Therefore, the stagnation-point velocity gradient on the sphere is

$$\frac{\beta D}{u_\infty} = \frac{3}{1 - 0.797\lambda^3} \tag{14}$$

If λ is small, there is very little effect on $\beta D/u_\infty$.

Compressibility Effect on Velocity Gradient

The effect of compressibility on the stagnation-point velocity gradient of a sphere in an infinite-diameter stream can be obtained by using the potential flow function in reference 3 that was derived by the Rayleigh-Janzen method

$$\varphi = \varphi_0 + \varphi_1 M_\infty^2 + \cdots \tag{15}$$

where terms of M_∞^4 and larger are neglected. A solution for the velocity at the surface of the sphere is given in reference 3 and may be used to express the nondimensional velocity gradient in the form that follows:

$$\frac{\beta D}{u_\infty} = 3 - 0.755 M_\infty^2 \tag{16}$$

Thus, the velocity gradient on a sphere in an infinite-diameter stream decreases as the Mach number increases as shown in figure 1. The experimental points that are shown from reference 9 were for a hemisphere in a bounded stream.

The compressibility effect on the potential flow function of a sphere in a circular cylinder of infinite length was obtained in reference 8 in the same manner as the solutions for the sphere in reference 3. By using the results of reference 8, the stagnation-point velocity gradient can be expressed for this type of configuration as follows:

$$\frac{\beta D}{u_\infty} = 3K + 2M_\infty^2 K^3\left[\left(0.531\lambda^3 + 0.333\right)K - 0.711\right] \tag{17}$$

where

$$K = \frac{1}{1 - 0.797\lambda^3} \tag{18}$$

For $\lambda = 0$, equation (17) reduces to equation (16).

Thus, from the preceding discussion, it appears possible to make a combined theoretical evaluation of the effect of shape, channel blocking, and compressibility on stagnation-point heat transfer in a subsonic stream.

Combined Effect of Shape, Channel Blocking, and Compressibility

Because the heat transfer is proportional to the square root of the stagnation-point velocity gradient, a relationship may be derived that combines the effects of shape, channel blocking, and compressibility in a subsonic bounded stream on the stagnation-point heat transfer. By combining equations (12) and (17) the following result is obtained:

$$\frac{\left(\dot{q}_s\right)_{M,\lambda,R_b/R_f}}{\left(\dot{q}_s\right)_{M=0,\lambda=0,R_b/R_f=1}} = \left(K\left\{1 + \frac{2}{3}M_\infty^2K^2\left[\left(0.531\lambda^3 + 0.333\right)K - 0.711\right]\right\}\right)^{0.5}\left(0.65 + 0.35\frac{R_b}{R_f}\right) \tag{19}$$

Equation (19) was normalized by using the stagnation-point heat transfer on a hemisphere at $M = 0$ in an infinite-diameter stream as a reference. In order to obtain equation (19) it was necessary to assume that the compressibility effect on the stagnation-point velocity gradient for other bodies is similar to that for a sphere. A representation of equation (19) is shown as a function of Mach number and the diameter ratio λ in figure 3. It can be seen in figure 3 that the stagnation-point heat-transfer rate increases with increasing λ and decreases with increasing Mach number for all values of λ.

Evaluation of Subsonic Stagnation-Point Heat Transfer in Tunnel Conditions

The general heat-transfer expression (eq. (3)) may be evaluated by expressin density and velocity in terms of pressure, temperature, flow rate of test medium, and cross-sectional area of the stream. The tunnel-wall boundary layer may be neglected in calculating the velocity in a low-subsonic stream because of the lo Reynolds number and the short length available for boundary-layer growth. The velocity may be assumed uniform and may be calculated by using the continuity equation:

$$u_\infty = \frac{\dot{w}}{\rho_\infty A} \tag{20}$$

The density for air can be determined from reference 10 and expressed as

$$\rho = 1.873 \times 10^{-2}\frac{p}{ZT} \tag{21}$$

The heat-transfer rate that is measured experimentally is an initial value base on a cold-wall temperature. In order to obtain initial theoretical heat-transf rates, an ambient wall temperature of 540° R and a Prandtl number of 0.71 were assumed and equation (21) was substituted for the necessary densities. Substituting equations (20) and (21) into equation (3) and simplifying, the initia

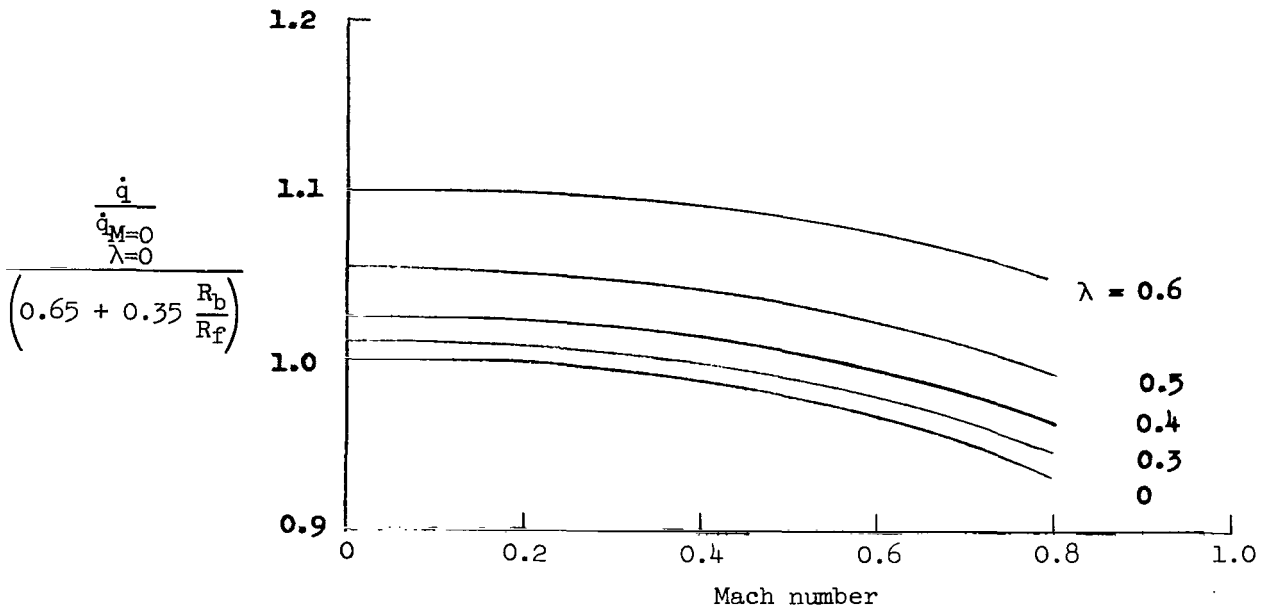

Figure 3.- Effect of blocking on the stagnation-point heat-transfer rate as a function of Mach number. $\lambda = \frac{\text{Model diameter}}{\text{Stream diameter}}$.

stagnation-point heat transfer on a body in a subsonic tunnel may be written as follows:

$$\dot{q}_s = 0.64\left(\frac{p_s}{p_\infty}\right)^{0.5} \frac{(Z_\infty T_\infty)^{0.5}}{(Z_s T_s)^{0.4}}\left(\frac{\beta D}{u_\infty}\right)^{0.5}\left(\frac{\dot{w}}{AD}\right)^{0.5}(\mu_s)^{0.4}(h_s - 125) \qquad (22)$$

In a low-subsonic stream, the ratios of free-stream pressure to stagnation pressure, and of free-stream temperature to stagnation temperature are approximately 1, therefore, the incompressible stagnation heat-transfer rate on a body in a low-subsonic equilibrium laminar stream may be written as

$$\dot{q}_s = 0.64(Z_\infty T_\infty)^{0.1}\left(\frac{\beta D}{u_\infty}\right)^{0.5}\left(\frac{\dot{w}}{AD}\right)^{0.5}(\mu_s)^{0.4}(h_s - 125) \qquad (23)$$

Equation (23) was derived from boundary-layer solutions; therefore, all radiation from the gas is neglected.

Equation (23) can be arranged in a form with all the temperature-dependent terms on the right-hand side as follows:

$$\frac{\dot{q}_s}{\left(\frac{\beta D}{u_\infty}\right)^{0.5}\left(\frac{\dot{w}}{AD}\right)^{0.5}} = 0.64(Z_\infty T_\infty)^{0.1}(\mu_s)^{0.4}(h_s - 125) \qquad (24)$$

The left-hand side of equation (24) is shown in figure 4 as a function of temperature, pressure, and enthalpy. The coefficient of viscosity was determined

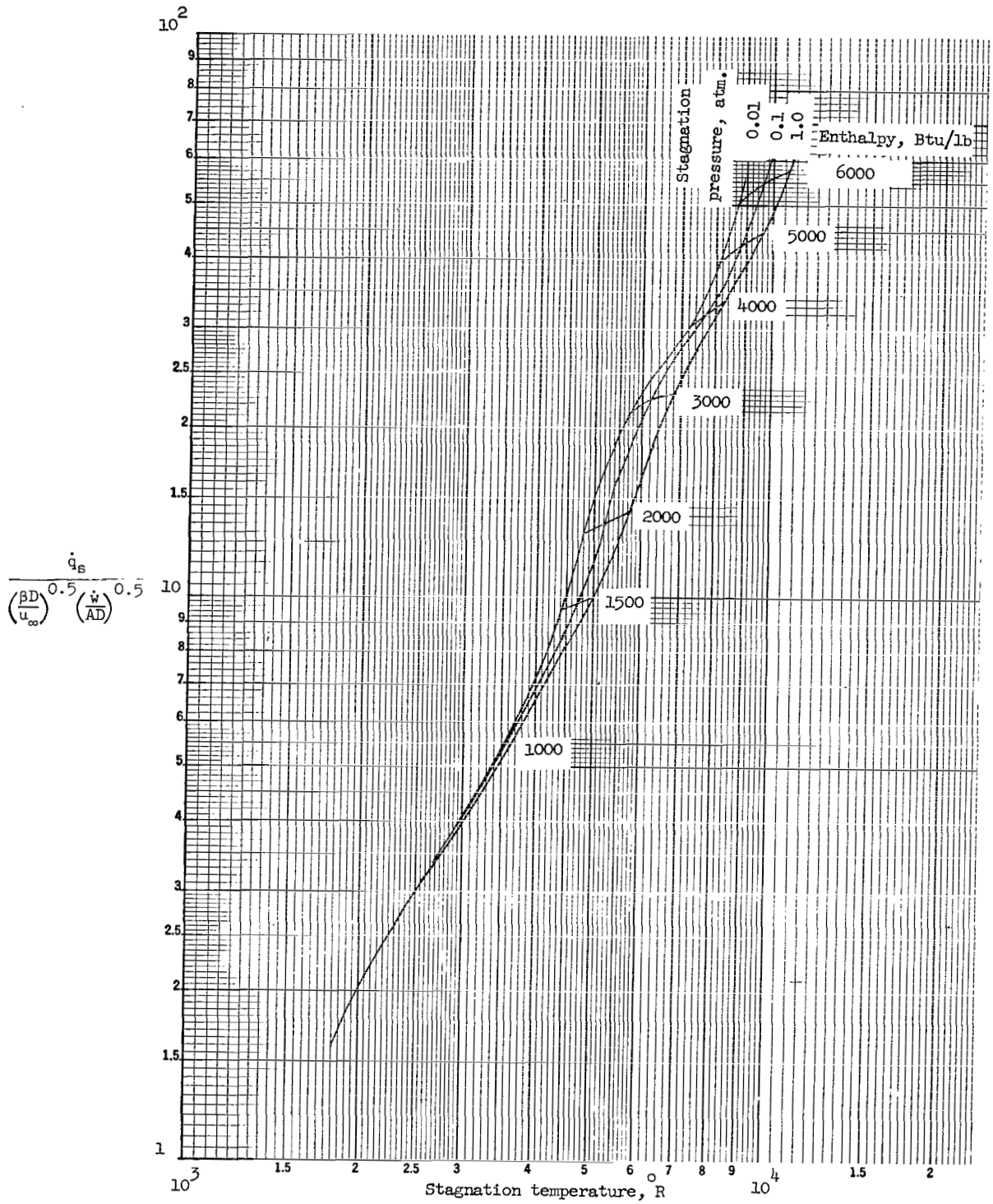

Figure 4.- Incompressible subsonic stagnation-point heat-transfer parameter as a function of temperature for various values of pressure and enthalpy.

from reference 11. Figure 4 may be used in conjunction with figures 2 and 3 to calculate the stagnation-point heat-transfer rate on a body in a subsonic equilibrium laminar flow stream.

APPARATUS, MODELS, AND PROCEDURE

6-Inch Subsonic Arc Tunnel

The 6-inch subsonic arc tunnel at the Langley Research Center is described in detail in reference 2. This arc tunnel shown in figure 5 is essentially a subsonic wind tunnel with a 6-inch axisymmetric test section, that utilizes a three-phase a-c water-cooled copper-electrode arc unit in the settling chamber to heat the air to temperatures up to 8,000° R. The arc unit consists of three pairs of electrodes that are equally spaced around the axis of the arc unit; each pair consists of two concentric water-cooled copper rings. Each 3-inch-diameter center electrode is connected to one phase of a three-phase a-c power supply, and the 6-inch-diameter outside electrodes are connected to the grounded neutral of the power supply. The arcs are rotated at about 360 rps by a magnetic field that is induced along the axis of the arc unit by a d-c electromagnetic coil in the plane of the electrodes. The arc rotation changes direction as the current goes from a positive to negative, as a result of the induced field of the arc combining with the constant direction field.

The air is passed through the arcing region, heated, and discharged through a 6-inch-diameter subsonic nozzle into a 6-inch-diameter graphite cylinder which is 1.25 diameters in length. The air proceeds into a 8-inch-diameter test section. The heat-transfer model was located on the center line of the tunnel

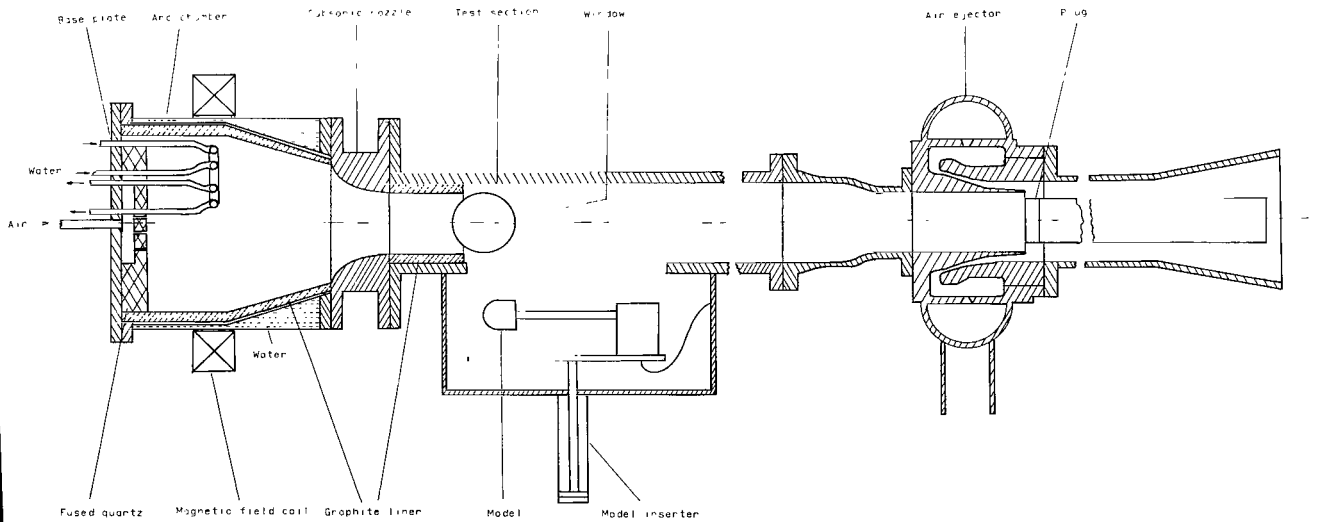

Figure 5.- Sketch of 6-inch subsonic arc tunnel.

$1\frac{1}{2}$ inches from the exit of the graphite-cylinder liner. This configuration is different from the theoretical model that was used for the channel-blocking-effect calculation. This type of configuration would have less channel-blocking effect because the flow could expand around the model more readily. The sting-supported model is mounted on a pneumatically operated door. (See fig. 5.) The model moves from the edge of the stream to within 1/4 inch of the center of the stream in 0.03 second. The "cushion" effect on the piston makes the total time from the edge to the center of stream about 0.16 second. An auxiliary air-operated ejector is used for a low-pressure reservoir to permit operation with a test-section pressure of less than atmospheric.

Heat-Transfer Models

A 3-inch-diameter flat-face 1/32-inch Inconel model (shown in fig. 6(a)) was used for determining the stagnation-point heat-transfer rate. The corner-radius ratio of the model (corner radius/model radius) is 0.0833. Thermocouples were located along the back surface of the model as shown in figure 6(a). The 2-inch- and 1-inch-diameter flat-face Inconel heat-transfer models are shown in figure 7, and locations are shown for the thermocouples. The 3-inch-diameter hemisphere-cylinder Inconel heat-transfer model with thermocouple locations are shown in figure 6(b). The material thickness was determined at each thermocouple location for each heat-transfer model before the thermocouple wire was installed. The individual thermocouple wires of No. 30 chromel-alumel were spotwelded 1/16 inch apart to the inside surface of the model.

MEASUREMENTS

Gas Temperature

The free-stream temperature at the test section was measured by the atomic-line-intensity ratio method by using the electronic excitation spectrum of the copper that appears in the gas from the small contamination caused by the electrodes. This temperature-measurement system is discussed in detail in reference 12. A simple medium glass spectrograph, with a 60° prism and an f-number 11.7 was used in conjunction with a photoelectric read-out system for recording the intensity ratio of the copper lines at 5153 A and 5700 A. The temperature (assuming thermodynamic equilibrium) is a function of this intensity ratio. The free-stream temperature was measured 1 inch forward of the stagnation point of the model in each test.

Heat-Transfer Rate

The heat-transfer rate at the stagnation point on the Inconel heat-transfer models was determined by using the temperature-rise rate through the material and neglecting lateral conduction terms. The heat-transfer rate is

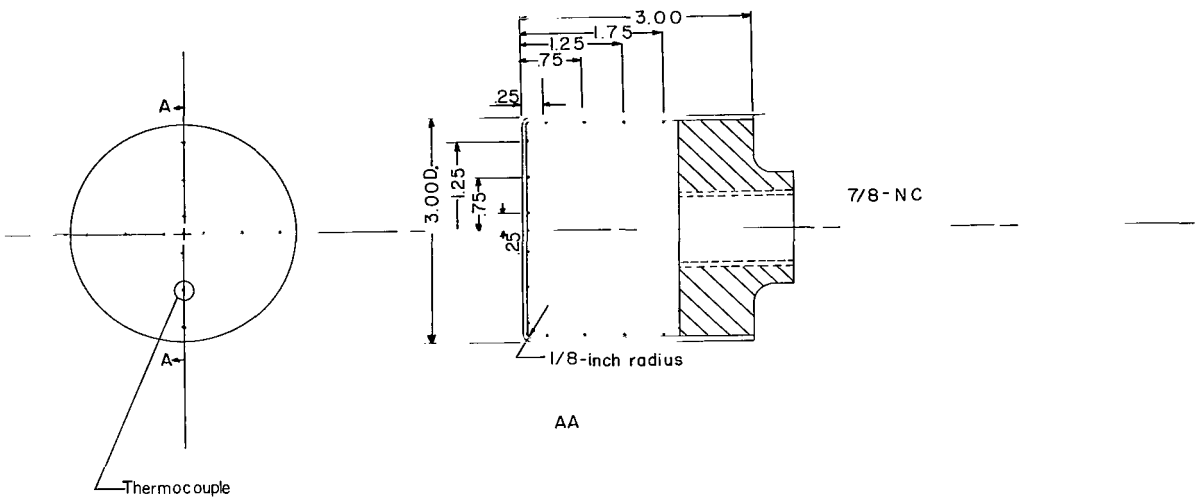

(a) Flat-face heat-transfer model; 1/32-inch Inconel.

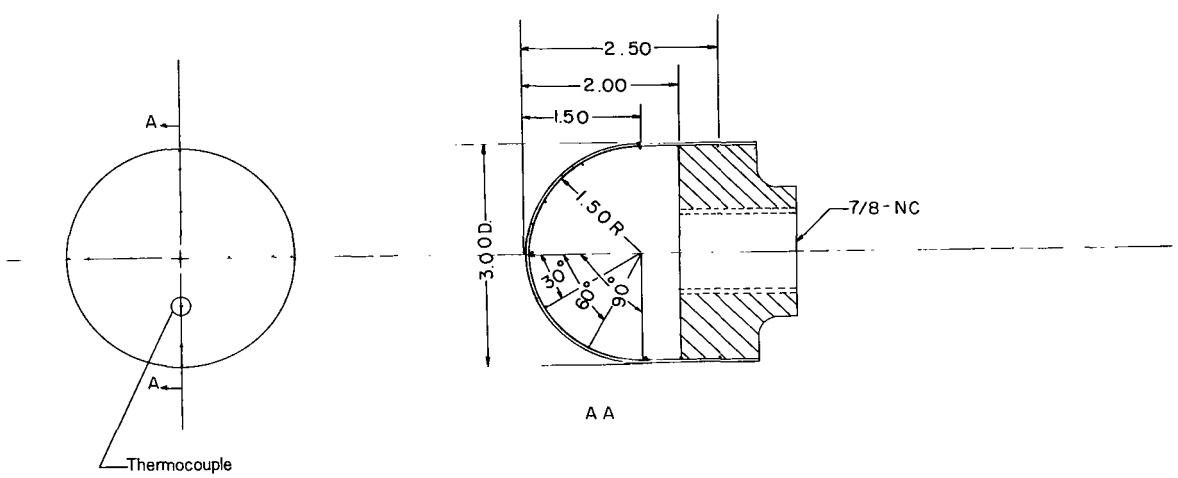

(b) Hemispherical heat-transfer model; 1/32-inch Inconel.

Figure 6.- Flat-face cylinder and hemisphere-cylinder heat-transfer models; 3-inch diameter.

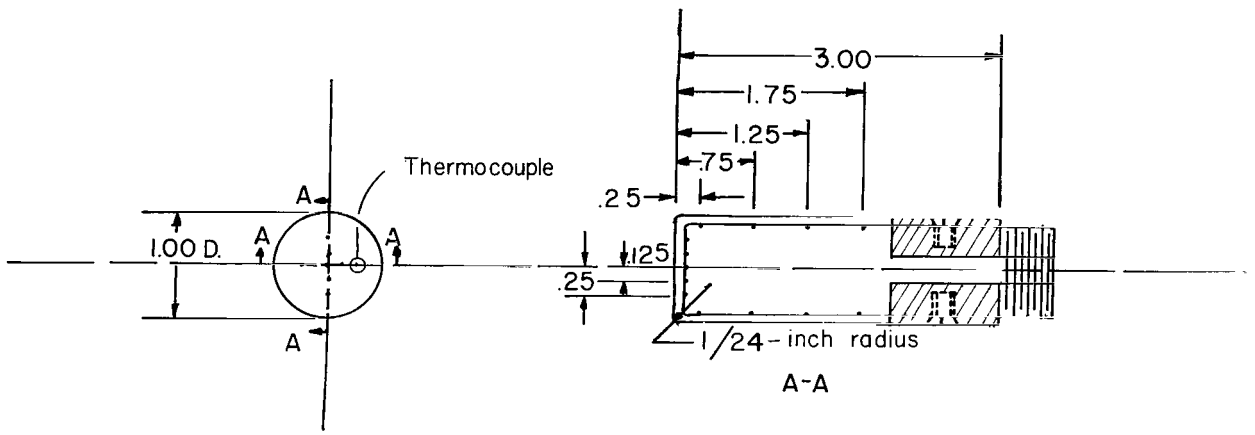

(a) 1-inch-diameter flat-face heat-transfer model; 1/32-inch Inconel.

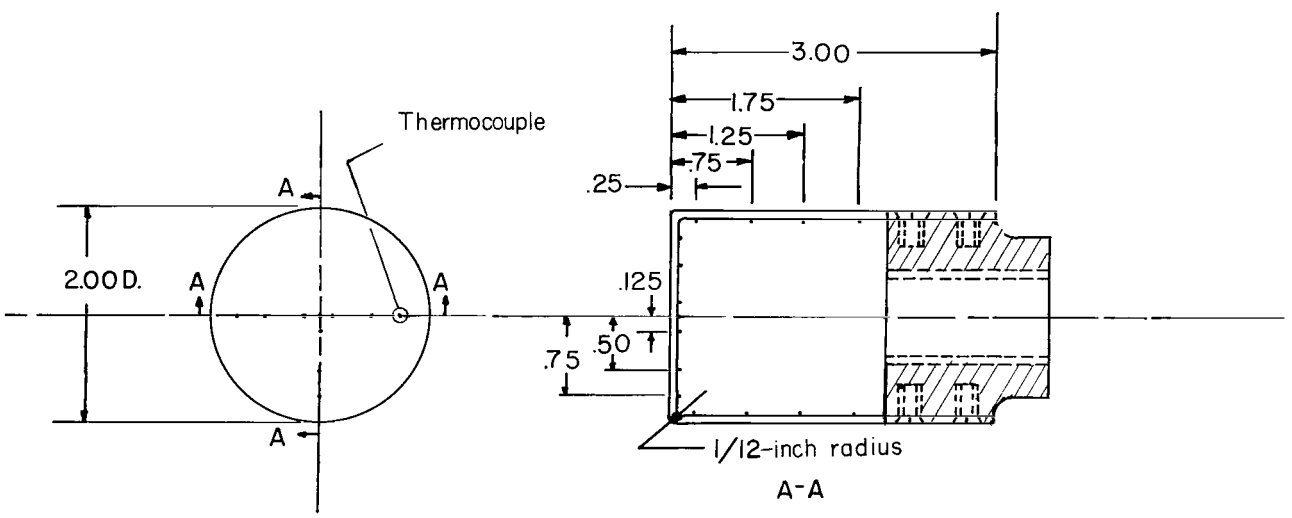

(b) 2-inch-diameter flat-face heat-transfer model; 1/32-inch Inconel.

Figure 7.- Flat-face-cylinder heat-transfer models; 1- and 2-inch diameter.

$$\dot{q}_s = c_p \rho \tau \frac{dT}{dt} \tag{25}$$

After a short time, the temperature-rise rate on the back surface is the same as that on the front surface. The temperature of the back surface of the material was recorded on an oscillograph. An initial slope of the temperature-time oscillograph trace was taken between temperatures where the specific heat of the material c_p is well known. The thickness τ and the density ρ can be determined with good accuracy. Therefore, the heat-transfer rate can be determined with the same precision as the slope of the back-surface temperature-time curve. Heat-transfer distributions can be obtained by using the thermocouples that are located along the inside surface of the models.

Test Procedure

The tunnel was started and brought to the desired tunnel flow rate. The heat-transfer models were inserted into the stream after steady operating conditions had been reached and then removed after 0.6 second. The short test time was necessary to assure model survival inasmuch as the temperature-rise rate was 1,500 deg/sec on some portions of the thin skin on the model. Heat-transfer rates, distributions, and free-stream temperatures were taken during each test as previously discussed. Three tunnel air-flow rates were used, and each tunnel air-flow rate was repeated several times with the 3-inch-diameter flat-face cylinder model to determine the reproducibility of heat-transfer measurements. Tests at the three tunnel flow rates were repeated at atmospheric pressure without operation of the air ejector. Heat-transfer rates were obtained on the 2-inch- and 1-inch-diameter flat-face cylinders and on the 3-inch-diameter hemisphere-cylinder for the same test conditions as the 3-inch-diameter flat-face cylinder.

TEST RESULTS AND DISCUSSION

The stagnation-point heat-transfer rate on the 3-inch-diameter flat-face-cylinder model reproduced within 2 percent of the average for four tests that were obtained at an air-flow rate of 0.08 lb/sec. The test conditions and measured stagnation-point heat-transfer rates for the various flat-face bodies and the 3-inch-diameter hemisphere are tabulated in the following table. There is little change (a percent or so) in the velocity gradient due to the small Mach number range of the tests. (See table.) Also, a blocking effect on the stagnation heat-transfer rate of approximately 5 percent is predicted theoretically for the 3-inch-diameter model in the 6-inch-diameter stream and the effect is even less for smaller bodies. (See fig. 3.) Unpublished pressure distributions on a 3-inch-diameter flat-face cylinder model in a 4-inch-diameter stream with a similar facility indicate that the channel-blocking effect on the stagnation velocity gradient is less than 10 percent. Therefore, the channel-blocking effect will be neglected. A comparison between the experimental stagnation-point heat-transfer measurements on the 3-inch- and 1-inch-diameter bodies and the theoretical calculations for the same type of bodies at a static pressure of

TABLE I

6-INCH SUBSONIC HIGH-TEMPERATURE ARC TUNNEL STAGNATION-POINT HEAT TRANSFER ON FLAT-FACE CYLINDERS AND HEMISPHERE CYLINDER

w, lb/sec	T, °R	p, atm	$\dot{q}$, Btu/sq ft-sec	D, in.	Model	M	N_{Re}	N_{St}
0.083	7,800	0.16	60.3	3	ff	0.15	1,650	0.0370
.138	7,900	.26	73.6	3	ff	.15	2,720	.0288
.218	6,700	.40	64.4	3	ff	.14	4,720	.0197
.084	6,600	1.0	39.1	3	ff	.02	1,850	.0348
.137	6,750	1.0	49.2	3	ff	.04	2,970	.0264
.214	6,600	1.0	53.0	3	ff	.05	4,870	.01845
.098	7,800	.16	90.5	2	ff	.15	1,300	.0463
.141	7,900	.26	94.6	2	ff	.15	1,855	.0363
.222	6,700	.40	91.9	2	ff	.14	3,090	.0275
.095	6,600	1.0	60.0	2	ff	.02	1,470	.0465
.155	6,750	1.0	63.6	2	ff	.04	2,240	.02985
.232	6,600	1.0	72.9	2	ff	.05	3,330	.0236
.085	7,800	.16	120.2	1	ff	.15	560	.0730
.134	7,900	.26	126.2	1	ff	.15	880	.0507
.210	6,700	.40	126.8	1	ff	.14	1,510	.0400
.085	6,600	1.0	78.0	1	ff	.02	625	.0685
.134	6,750	1.0	93.8	1	ff	.04	970	.0510
.210	6,600	1.0	105.5	1	ff	.05	1,580	.0359
.083	7,800	.16	97.1	3	hs	.15	1,650	.059
.147	7,900	.26	123.0	3	hs	.15	2,900	.045
.266	6,700	.40	120.0	3	hs	.14	5,750	.0310
.098	6,600	1.0	78.6	3	hs	.02	2,160	.0593
.148	6,750	1.0	85.0	3	hs	.04	3,210	.0416
.222	6,600	1.0	100.0	3	hs	.05	5,050	.0346

l atmosphere is shown in figure 8 as a function of tunnel air-flow rate. It is shown in figure 8 that the experimental heat transfer for the 1-inch-diameter body is approximately 40 percent greater than the theoretical value at a tunnel air-flow rate of 0.08 lb/sec. On the 3-inch-diameter body, the experimental heat transfer is approximately 20 percent greater than the theoretical value at the same flow rate.

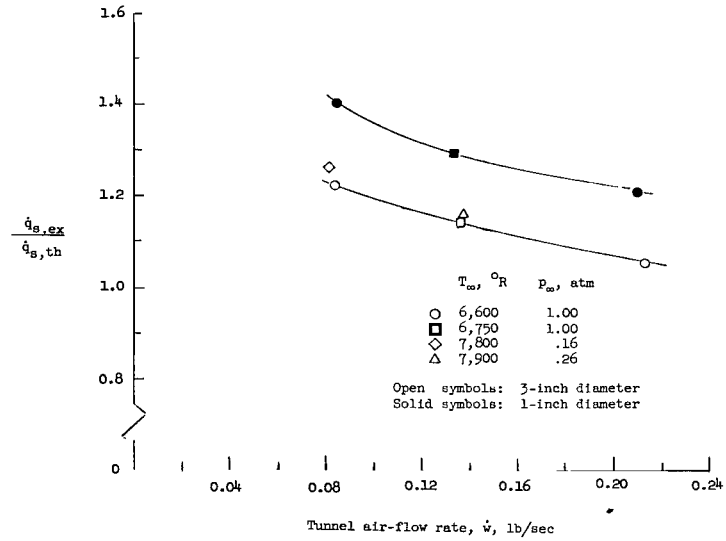

Figure 8.- Ratio of experimental to theoretical stagnation-point heat transfer to flat-face cylinders.

The difference between theoretical and experimental stagnation heat transfer may possibly be attributed to departure from three simplifying assumptions.

1. No Radiation - Radiative heat transfer to the model could come from the large quantity of hot gas ahead of the model and from the electric arcs in the arc chamber.

2. Equilibrium Flow - The flow at the low pressures (0.16 and 0.26 atm) may not be in equilibrium as discussed in reference 13.

3. Laminar Flow - The disturbances of the rotation and continuous restriking of the a-c arcs may cause free-stream turbulence that would give a deviation from laminar-flow theory.

The total radiation from the electric arcs and hot-gas stream would give a radiant heat-transfer rate that would be independent of model diameter. For the 3-inch-diameter model at atmospheric pressure, the difference between theory and experiment is 8 Btu/sq ft-sec at the low tunnel air-flow rate. On the 1-inch-diameter model, the difference at the low flow rate was 26 Btu/sq ft-sec. A heat-transfer probe that would separate the radiant from the convective heat transfer in a similar facility indicated the radiant heat transfer to be less than 2 percent of the total heat transfer. Therefore, it can be concluded that the difference cannot be attributed entirely to radiation.

Additional experimental points are shown in figure 8 for the 3-inch-diameter model at pressure levels and temperatures that could have nonequilibrium flow according to reference 13. However, all of heat-transfer surfaces were of the same type material (Inconel). The walls of all of the three different-diameter models were thus expected to be catalytic so that recombination would occur at the model surface. It should be noted that the heat-transfer data differed approximately the same amount from theory for all the temperature and pressure conditions at the same tunnel air-flow rate (fig. 8). It is believed that the

flow is in equilibrium at atmospheric pressure and 6,700° R (ref. 13). Therefore, it may be concluded that the difference between theory and experiment cannot be attributed entirely to a nonequilibrium condition.

Stagnation-point Stanton numbers were calculated from the stagnation-point heat transfer, the free-stream temperature, and the tunnel flow rate measurements and are plotted against Reynolds number based on body diameter in figure 9. The Fay and Riddell Stanton number (eq. (5)) is shown in the same figure with several free-stream temperatures. A straight line was faired through the points taken at 6,700° R because these points gave the largest Reynolds number variation. Additional points taken at approximately 7,900° R are also shown. Since the Fay and Riddell Stanton number (eq. (5)) is independent of pressure, the 6,700° R points were plotted without regard to pressure level. The experimental data can be represented in the same form as the Fay and Riddell Stanton number by using

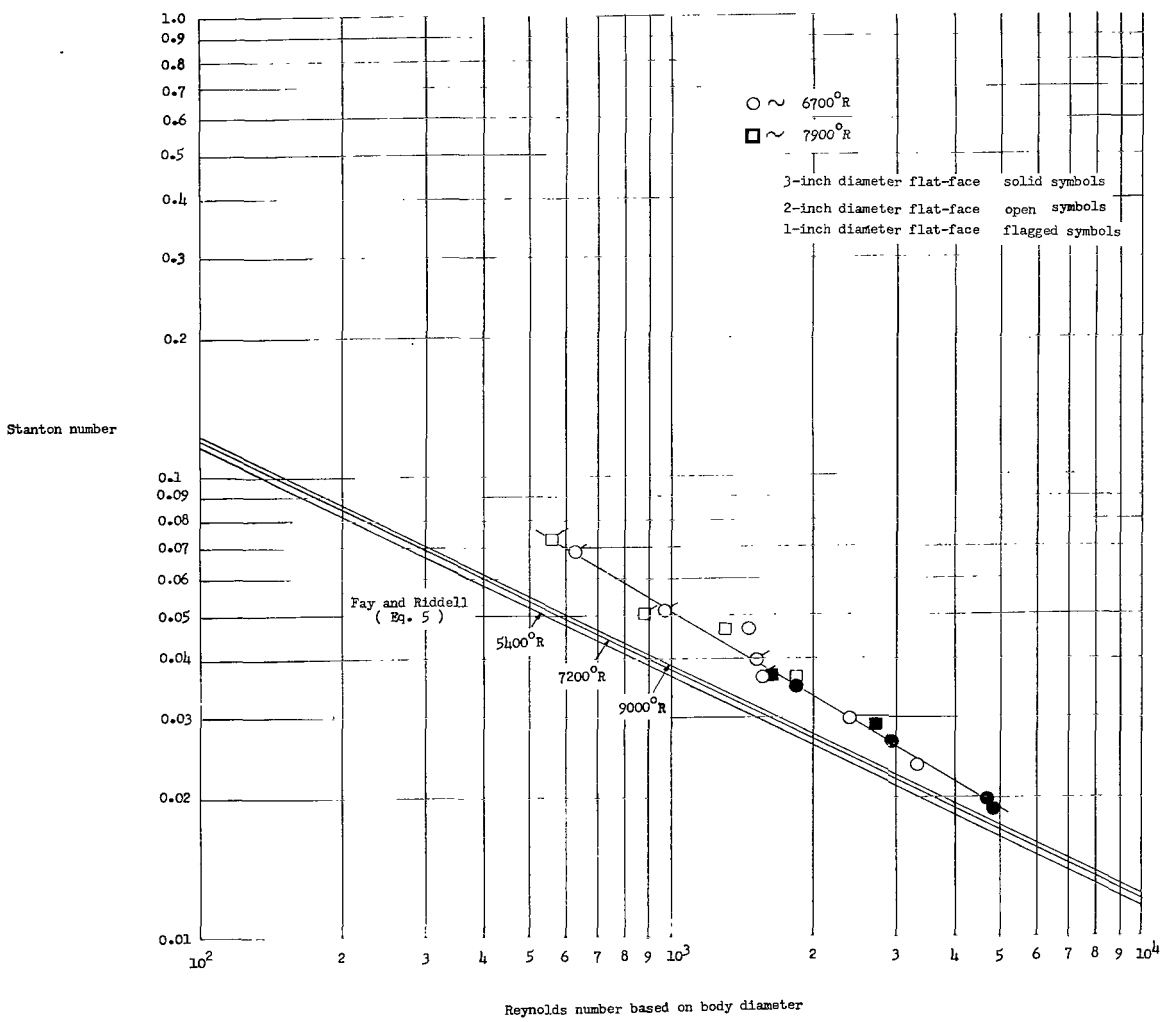

Figure 9.- Experimental and theoretical Stanton number as a function of Reynolds number.

the theoretical velocity gradients and evaluating the exponents and the constant by using the experimental data. Such a representation is as follows:

$$N_{St,s} = 3.17\left(\frac{\beta D}{u_\infty}\right)^{0.64}\left(N_{Re}\right)^{-0.625}$$

Of the 24 test conditions, 22 fall within 5 percent of the empirical equation and all are within 10 percent. It can be noted, by extrapolating the faired line on the Stanton number plot, that in the Reynolds number region of 10,000, the experimental Stanton number approaches the Fay and Riddell solutions.

The fact that the empirical Stanton number exponents are different from the laminar-equilibrium flow Stanton number is attributed to the turbulent free-stream state of the test medium. That is, the three electric a-c arcs that are used to heat the air to the desired enthalpy level impart a considerable amount of turbulence to the air because the arcs are extinguished, re-ignited, and change rotational direction on each half cycle. The rotational speed of each arc is approximately 360 rps.

A heat-transfer distribution is shown in figure 10 for the 3-inch-diameter flat-face body. The heat-transfer distributions were similar for the 1- and 2-inch-diameter bodies. A theoretical distribution for a similar body (from ref. 14) is shown for comparison at a supersonic Mach number. The similarity is probably a function of a turbulent transition in the stream at the subsonic Mach number. A measured heat-transfer distribution on the 3-inch-diameter hemisphere and a theoretical distribution at supersonic Mach numbers from reference 15 is shown in figure 11. The experimental distribution on the hemisphere is quite similar to the distribution in reference 16 that assumes a turbulent transition. The heat-transfer distribution on a body is strictly a local problem. In the supersonic case of a hemisphere, the flow expands from the stagnation point and passes through a sonic point approximately 45°

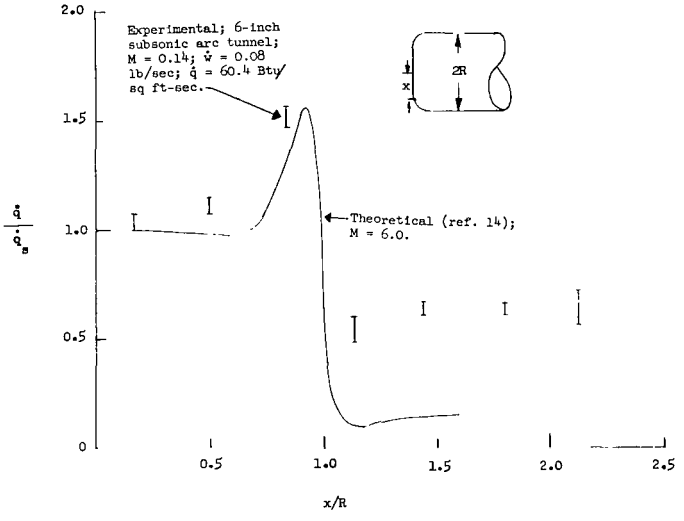

Figure 10.- Heat-transfer distribution on a 3-inch-diameter flat-face model.

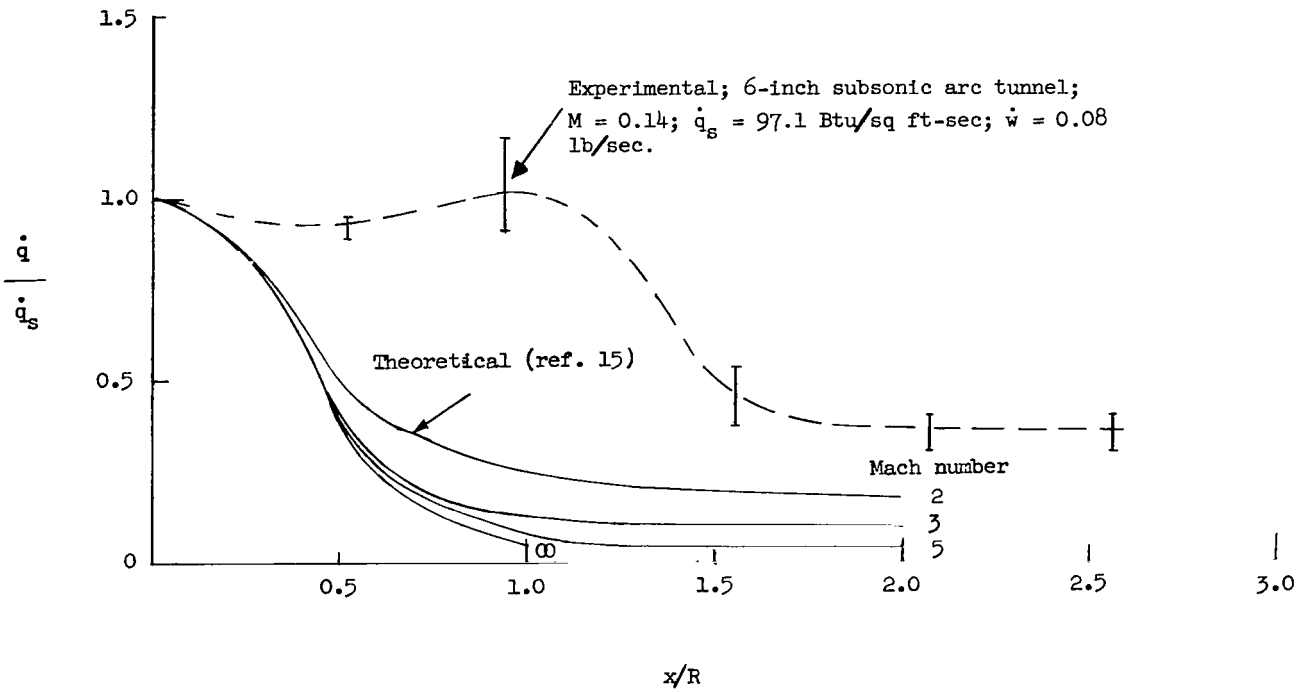

Figure 11.- Heat-transfer distribution on a hemisphere-cylinder.

from the stagnation point. However, in a subsonic stream there is very little change in the density and velocity along the surface of the model. Therefore, any heat-transfer distribution such as that shown in figures 10 and 11 would have to be due to a change in the local Stanton number. This could be the result of a transition due to the free-stream turbulence which is caused by the arcs that heat the test medium.

In reference 17, stagnation-point heat-transfer measurements are used to calculate enthalpies for correlating ablation data in a Mach 2 arc jet. This same approach cannot be used in a subsonic arc facility unless it is known that the flow is laminar, in equilibrium, and that there is no radiant heat transfer. Enthalpies calculated from heat-transfer measurements in the subsonic facility described in reference 2 would be much greater than those measured with the spectrometric method described herein.

CONCLUSIONS

Stagnation-point heat-transfer measurements on flat-face cylinders of three different diameters in a 6-inch subsonic arc tunnel do not follow the laminar heat-transfer theory of Fay and Riddell for the Reynolds number range covered in this report. It was concluded that the difference between theory and experiment

was not a function of velocity-gradient variation because of compressibility or channel-blocking effects. The deviation from laminar-flow theory is attributed to the free-stream turbulence in the test medium that is caused by the a-c electric arcs in the arc chamber of the subsonic arc tunnel.

Langley Research Center,
National Aeronautics and Space Administration,
Langley Station, Hampton, Va., April 26, 1963.

REFERENCES

1. Fay, J. A., and Riddell, F. R.: Theory of Stagnation Point Heat Transfer in Dissociated Air. Jour. Aero. Sci., vol. 25, no. 2, Feb. 1958, pp. 73-85, 121.

2. Brown, Ronald D., and Levin, L. Ross: A 6-Inch Subsonic High-Temperature Arc Tunnel for Structures and Materials Tests. NASA TN D-1621, 1963.

3. Kaplan, Carl: The Flow of a Compressible Fluid Past a Sphere. NACA TN 762, 1940.

4. Milne-Thompson, L. M.: Theoretical Hydrodynamics. Second ed., The Macmillan Co., 1950, p. 425.

5. Curtiss, H. A., and Pneuman, G. W.: Experimental Determination of Stagnation Point Velocity Gradient on a Right Circular Cylinder in a Subsonic Free Jet. RAD Tech. Memo. 2-TM-58-106, AVCO Res. and Advanced Dev. Div., Oct. 9, 1958.

6. Stoney, William E., Jr.: Aerodynamic Heating of Blunt Nose Shapes at Mach Numbers up to 14. NACA RM L58E05a, 1958.

7. Haberman, William L.: Subsonic Potential Flow Past a Sphere Inside a Cylindrical Duct. Jour. Aerospace Sci. (Readers' Forum), vol. 29, no. 3, Mar. 1962, pp. 356-357.

8. Haberman, W. L.: The Potential Problem of a Sphere Inside a Circular Cylinder. Rep. 1563, David Taylor Model Basin, Navy Dept., Oct. 1961.

9. Korobkin, Irving: Laminar Heat Transfer Characteristics of a Hemisphere for the Mach Number Range 1.9 to 4.9. NAVORD Rep. 3841 (Aeroballistic Res. Rep. 257), U.S. Naval Ord. Lab. (White Oak, Md.), Oct. 10, 1954.

10. Moeckel, W. E., and Weston, Kenneth C.: Composition and Thermodynamic Properties of Air in Chemical Equilibrium. NACA TN 4265, 1958.

11. Hansen, C. Frederick: Approximations for the Thermodynamic and Transport Properties of High-Temperature Air. NASA TR R-50, 1959. (Supersedes NACA TN 4150.)

12. Pearce, Willard J.: Plasma Jet Temperature Study. WADC Tech. Rep. 59-346 (Contract No. AF 33(616)-5848), U.S. Air Force, Feb. 1960.

13. Winkler, Ernest L., and Griffin, Roy N., Jr.: Measurements in a Frozen, Partially Dissociated, High-Speed Gas Stream. Advances in Hypervelocity Techniques, Arthur M. Krill, ed., Plenum Press (New York), 1962, pp. 511-522.

14. Beckwith, Ivan E., and Cohen, Nathaniel B.: Application of Similar Solutions to Calculation of Laminar Heat Transfer on Bodies With Yaw and Large Pressure Gradient in High-Speed Flow. NASA TN D-625, 1961.

15. Hanawalt, A. J., Blessing, A. H., and Schmidt, C. M.: Thermal Analysis of Stagnation Regions With Emphasis on Heat-Sustaining Nose Shapes at Hypersonic Speed. Jour. Aero/Space Sci., vol. 26, no. 5, May 1959, pp. 257-263.

16. Van Driest, E. R.: Convective Heat Transfer in Gases. Turbulent Flows and Heat Transfer. Vol. 5 of High Speed Aerodynamics and Jet Propulsion, sec. F,13, C. C. Lin, ed., Princeton Univ. Press, 1959, pp. 388-390.

17. Chapman, Andrew J.: An Experimental Investigation of Several Ablation Materials in an Electric-Arc-Heated Air Jet. NASA TN D-1520, 1963.

"The aeronautical and space activities of the United States shall be conducted so as to contribute . . . to the expansion of human knowledge of phenomena in the atmosphere and space. The Administration shall provide for the widest practicable and appropriate dissemination of information concerning its activities and the results thereof."

—NATIONAL AERONAUTICS AND SPACE ACT OF 1958

NASA SCIENTIFIC AND TECHNICAL PUBLICATIONS

TECHNICAL REPORTS: Scientific and technical information considered important, complete, and a lasting contribution to existing knowledge.

TECHNICAL NOTES: Information less broad in scope but nevertheless of importance as a contribution to existing knowledge.

TECHNICAL MEMORANDUMS: Information receiving limited distribution because of preliminary data, security classification, or other reasons.

CONTRACTOR REPORTS: Technical information generated in connection with a NASA contract or grant and released under NASA auspices.

TECHNICAL TRANSLATIONS: Information published in a foreign language considered to merit NASA distribution in English.

TECHNICAL REPRINTS: Information derived from NASA activities and initially published in the form of journal articles.

SPECIAL PUBLICATIONS: Information derived from or of value to NASA activities but not necessarily reporting the results of individual NASA-programmed scientific efforts. Publications include conference proceedings, monographs, data compilations, handbooks, sourcebooks, and special bibliographies.

Details on the availability of these publications may be obtained from:

SCIENTIFIC AND TECHNICAL INFORMATION DIVISION

NATIONAL AERONAUTICS AND SPACE ADMINISTRATION

Washington, D.C. 20546